Simulation Studies of Two-Stream Instability in Intense Particle Beams Based on Vlasov-Maxwell Equations

Hong Qin, Ronald C. Davidson, Edward Startsev, W. Wei-li Lee

Plasma Physics Laboratory
Princeton University

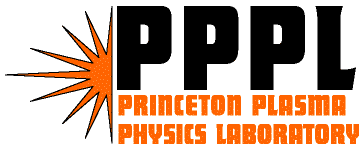

Presented at the International Workshop on Two-Stream Instabilities in Particle Accelerators and Storage Rings

September 11 –14, 2001

KEK, Tsukuba, Japan.

---

* Research supported by the U.S. Department of Energy and Spallation Neutron Source Project. We thank R. Macek, T.-S. Wang, P. Channell, K. Harkay, and M. Blaskiewicz for productive discussions and comments.

Outline

- Why the Vlasov-Maxwell Equations?
- The physics of two-stream instability and other collective effects.
- Theoretical model.
- Nonlinear δf particle simulation method and BEST code.
- Collective mode excitations.
- Simulations of e-p two-stream instabilities.
- Future work and conclusions.

Motivations

- For high intensity beam, it is increasingly important to develop an improved theoretical understanding of the influence of the intense self fields using a kinetic model based on the nonlinear Vlasov-Maxwell equations.
  - ✓ Space charge effects and collective instabilities.
  - ✓ Collective mode structures, growth rates, and thresholds.
  - ✓ Damping mechanisms and wave-particle interaction.
- 3D multi-species nonlinear δf particle simulation code based on nonlinear Vlasov-Maxwell equations provides an effective tool for the investigating collective processes. Space charge effects and collective instabilities.
  - ✓ Significantly reduced simulation noise.
  - ✓ Linear instability and nonlinear properties.

Why the Maxwell Equations

- For high intensity beams, the complete space charge impedance is a 3D Green's function depending on (z, a, m).
- For the study of collective instabilities in high intensity beams, the $\delta(z)$ and $\delta(a)$ expansions of source for the space charge impedance are less efficient, both analytically and numerically.
- Solving the Maxwell equations is more straightforward and analytically relevant. Numerically, more efficient expansions are often used.

Why the Vlasov Equation

- For collective instabilities, damping mechanisms are important in determining the growth rates and thresholds.
  - ✓ For the e-p instability in PSR, the macro-particle model predicts a growth rate 3000 times larger than the experimental value.
- Besides the conventional Landau damping, other important damping mechanisms include:
  - ✓ Longitudinal Landau damping due to momentum spread.
  - ✓ Damping due to space charge induced tune spread.
- Important physics of wave-particle interaction.
  - ✓ Landau damping induced emittance grow.
  - ✓ Wave-particle interaction induces halo particles.

Physics of Collective Instabilities

- Collective instabilities are the results of energy exchange between different degrees of freedom in systems with high beam intensities.
  - ✓ e-p instability: energy exchange between protons and electrons.
  - ✓ Pressure anisotropy instability (non-equal-partition mode): energy exchange between longitudinal and transverse direction.
- Energy exchange is mediated by the collective eigenmodes (excitations) existing in the system:
  - ✓ e-p instability: plasma oscillations of protons and electrons.
  - ✓ Pressure anisotropy instability (non-equal-partition mode): longitudinal (L1) and transverse (T2) eigenmodes .

Physics of Collective Instabilities

- Analytically, instabilities happen when the eigen frequencies of different eigenmodes cross each other.
  - ✓ e-p instability: $\omega_e=\omega_p+k_zV_b$.
  - ✓ Pressure anisotropy instability: $\omega_{T2}=\omega_{L1}$.

Two-Stream Instability for Intense Ion Beams

- In the absence of background electrons, an intense nonneutral ion beam supports collective oscillations (plasma oscillations) with phase velocity ω/k_z upshifted and downshifted relative to the average beam velocity $\beta_b c$.

- Introduction of an (unwanted) electron component (produced, for example, by secondary emission of electrons due to the interaction of halo ions with the chamber wall) provides the free energy to drive the classical two-stream instability.

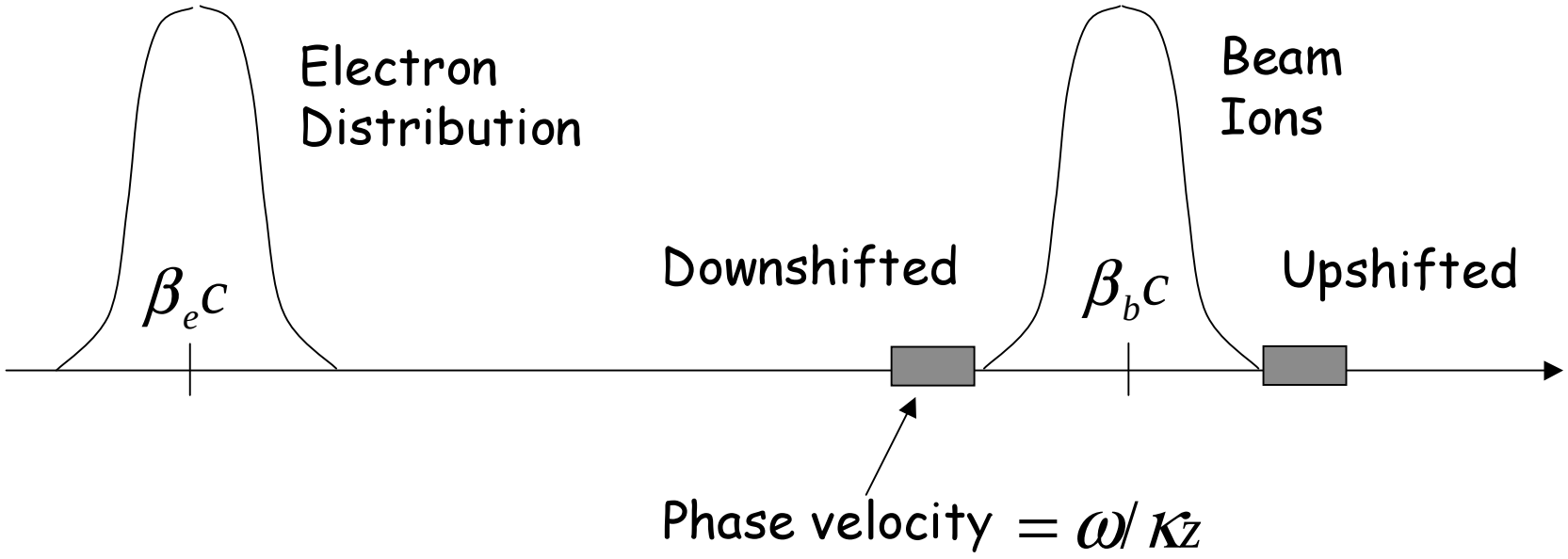

Two-Stream Instability for Intense Ion Beam

- Unlike the two-stream instability in a homogeneous neutral plasma, the two-stream instability for an intense, thin ion beam depends strongly on:
  - Transverse dynamics and geometry (r_b/r_w, $k_z r_b$).
  - Degree of charge neutralization ($f = \hat{n}_e/\hat{n}_b$).
  - Spread in transverse betatron frequencies.
  - Axial momentum spread.
- Strong experimental evidence for two-species instabilities:
  - Proton Storage Ring (PSR) at Los Alamos National Laboratory.
  - Beam-ion instability in electron machines.
  - Electron cloud instability in hadron machines.

Motivation

- Understand two-stream interaction process in high-intensity ion beams, and identify optimum operating regimes for:
  - Spallation Neutron Sources and Proton Storage Ring at LANL.
  - Hadron colliders.
  - Heavy ion fusion.
- For accelerator applications with high beam currents and charge densities, it is increasingly important to develop an improved theoretical understanding of the influence of the intense self fields using a kinetic model based on the nonlinear Vlasov-Maxwell equations.
- 3D multi-species nonlinear δf particle simulation code based on nonlinear Vlasov-Maxwell equations provides an effective tool for investigating collective processes.

Theoretical Model — Nonlinear Vlasov-Maxwell System

- Thin, continuous, high-intensity ion beam ($j = b$) propagates in the z-direction through background electron and ion components ($j = e, i$) described by distribution function $f_j(\boldsymbol{x}, \boldsymbol{p}, t)$.

- Transverse and axial particle velocities in a frame of reference moving with axial velocity $\beta_j c\hat{\boldsymbol{e}}_z$ are assumed to be *nonrelativistic*.

- Adopt a *smooth-focusing* model in which the focusing force is described by

$$\boldsymbol{F}_j^{foc} = -\gamma_j m_j \omega_{\beta j}^2 \boldsymbol{x}_\perp$$

- Self-electric and self-magnetic fields are expressed as $\boldsymbol{E}^s = -\nabla\phi(\boldsymbol{x}, t)$ and $\boldsymbol{B}^s = \nabla \times A_z(\boldsymbol{x}, t)\hat{\boldsymbol{e}}_z$.

Theoretical Model — Nonlinear Vlasov-Maxwell System

- Distribution functions and electromagnetic fields are described self-consistently by the nonlinear Vlasov-Maxwell equations in the six-dimensional phase space $(\boldsymbol{x}, \boldsymbol{p})$:

$$\left\{\frac{\partial}{\partial t} + \boldsymbol{v}\cdot\frac{\partial}{\partial \boldsymbol{x}} - [\gamma_j m_j \omega_{\beta j}^2 \boldsymbol{x}_\perp + e_j(\nabla\phi - \frac{v_z}{c}\nabla_\perp A_z)]\cdot\frac{\partial}{\partial \boldsymbol{p}}\right\} f_j(\boldsymbol{x},\boldsymbol{p},t) = 0$$

and

$$\begin{aligned}
\nabla^2\phi &= -4\pi\sum_j e_j \int d^3p f_j(\boldsymbol{x},\boldsymbol{p},t) \\
\nabla^2 A_z &= -\frac{4\pi}{c}\sum_j e_j \int d^3p v_z f_j(\boldsymbol{x},\boldsymbol{p},t)
\end{aligned}$$

Nonlinear δf Particle Simulation Method

- Divide the distribution function into two parts: $f_j = f_{j0} + \delta f_j$.
- f_{j0} is a known solution to the nonlinear Vlasov-Maxwell equations.
- Determine numerically the evolution of the perturbed distribution function $\delta f_j \equiv f_j - f_{j0}$.
- Advance the weight function defined by $w_j \equiv \delta f_j / f_j$, together with the particles' positions and momenta.
- Equations of motion for the particles are given by

$$\begin{aligned}
\frac{d\boldsymbol{x}_{\perp ji}}{dt} &= (\gamma_j m_j)^{-1} \boldsymbol{p}_{\perp ji}, \\
\frac{dz_{ji}}{dt} &= v_{zji} = \beta_j c + \gamma_j^{-3} m_j^{-1} (p_{zji} - \gamma_j m_j \beta_j c), \\
\frac{d\boldsymbol{p}_{ji}}{dt} &= -\gamma_j m_j \omega_{\beta j}^2 \boldsymbol{x}_{\perp ji} - e_j (\nabla\phi - \frac{v_{zji}}{c} \nabla_\perp A_z)
\end{aligned}$$

- Weight functions w_j are carried by the simulation particles, and the dynamical equations for w_j are derived from the definition of w_j and the Vlasov equation.

Nonlinear δf Particle Simulation Method

- Weight functions evolve according to

$$\begin{aligned} \frac{dw_{ji}}{dt} &= -(1-w_{ji})\frac{1}{f_{j0}}\frac{\partial f_{j0}}{\partial \boldsymbol{p}}\cdot\delta\Big(\frac{d\boldsymbol{p}_{ji}}{dt}\Big) \\ \delta\Big(\frac{d\boldsymbol{p}_{ji}}{dt}\Big) &\equiv -e_j(\nabla\delta\phi - \frac{v_{zji}}{c}\nabla_\perp\delta A_z) \end{aligned}$$

Here, $\delta\phi = \phi - \phi_0$, $\delta A_z = A_z - A_{z0}$, and $(\phi_0,\ A_{z0},\ f_{j0}\ )$ are the equilibrium solutions.

- The perturbed distribution function δf_j is given by the weighted Klimontovich representation

$$\delta f_j = \frac{N_j}{N_{sj}}\sum_{i=1}^{N_{sj}} w_{ji}\delta(\boldsymbol{x}-\boldsymbol{x}_{ji})\delta(\boldsymbol{p}-\boldsymbol{p}_{ji})$$

where N_j is the total number of actual j'th species particles, and N_{sj} is the total number of *simulation* particles for the j'th species.

Nonlinear δf Particle Simulation Method

- Maxwell's equations are also expressed in terms of the perturbed quantities:

$$\nabla^2 \delta\phi = -4\pi \sum_j e_j \delta n_j$$

$$\nabla^2 \delta A_z = -\frac{4\pi}{c} \sum_j \delta j_{zj}$$

$$\delta n_j = \int d^3p \delta f_j(\boldsymbol{x}, \boldsymbol{p}, t) = \frac{N_j}{N_{sj}} \sum_{i=1}^{N_{sj}} w_{ji} S(\boldsymbol{x} - \boldsymbol{x}_{ji})$$

$$\delta j_{zj} = e_j \int d^3p v_z \delta f_j(\boldsymbol{x}, \boldsymbol{p}, t) = \frac{e_j N_j}{N_{sj}} \sum_{i=1}^{N_{sj}} v_{zji} w_{ji} S(\boldsymbol{x} - \boldsymbol{x}_{ji})$$

where $S(\boldsymbol{x} - \boldsymbol{x}_{ji})$ represents the method of distributing particles on the grids.

Advantages of the δf method

- Simulation noise is reduced significantly.
  - Statistical noise $\sim 1/\sqrt{N_s}$.
  - To achieve the same accuracy, number of simulation particles required by the δf method is only $(\delta f/f)^2$ times of that required by the conventional PIC method.
- No waste of computing resource on something already known — f_0.
- Moreover, make use of the known (f_0) to determine the unknown (δf).
- Study physics effects separately, as well as simultaneously.
- Easily switched between linear and nonlinear operation.

The BEST Code

Application of the 3D multispecies nonlinear δf simulation method to PSR is carried out using the Beam Equilibrium Stability and Transport (BEST) code at the Princeton Plasma Physics Laboratory.

- Adiabatic field pusher for light particles (electrons).
- Solves Maxwell's equations in cylindrical geometry.
- Written in Fortran 90/95 and extensively object-oriented.
- NetCDF data format for large-scale diagnostics and visualization.
- Achieved an average speed of 40μs/(particle$\times$step) on a DEC alpha personal workstation 500au computer.
- The code has been parallelized using OpenMP and MPI.
  - NERSC: IBM-SP2 Processors.
  - PPPL: Dec-α Processors.
- Achieved 2.0×10^{10} ion-steps + 4×10^{11} electron-steps for instability studies.

Nonlinear Properties of Equilibrium Proton Beam

- Single-species thermal equilibrium ion beam in a constant focusing field.
- Equilibrium properties depend on the radial coordinate $r = (x^2 + y^2)^{1/2}$.
- Cylindrical chamber with perfectly conducting wall located at $r = r_w$.
- Thermal equilibrium distribution function for the beam ion is given by

$$f_{b0}(r, \boldsymbol{p}) = \frac{\hat{n}_b}{(2\pi\gamma_b m_b T_b)^{3/2}} \exp\left\{-\frac{H_\perp}{T_b}\right\} \times \exp\left\{-\frac{(p_z - \gamma_b m_b \beta_b c)^2}{2\gamma_b^3 m_b T_b}\right\}$$

- As a benchmark test, system parameters are chosen to correspond to high-intensity proton beam in PSR in the absence of background electrons.

Nonlinear Properties of Stable Proton Beam Propagation

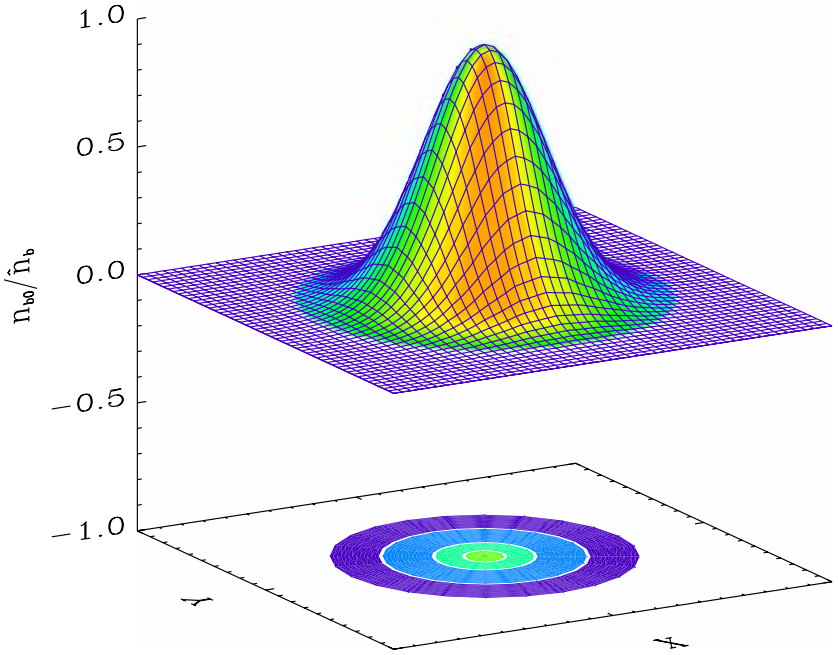

(a) Equilibrium Density

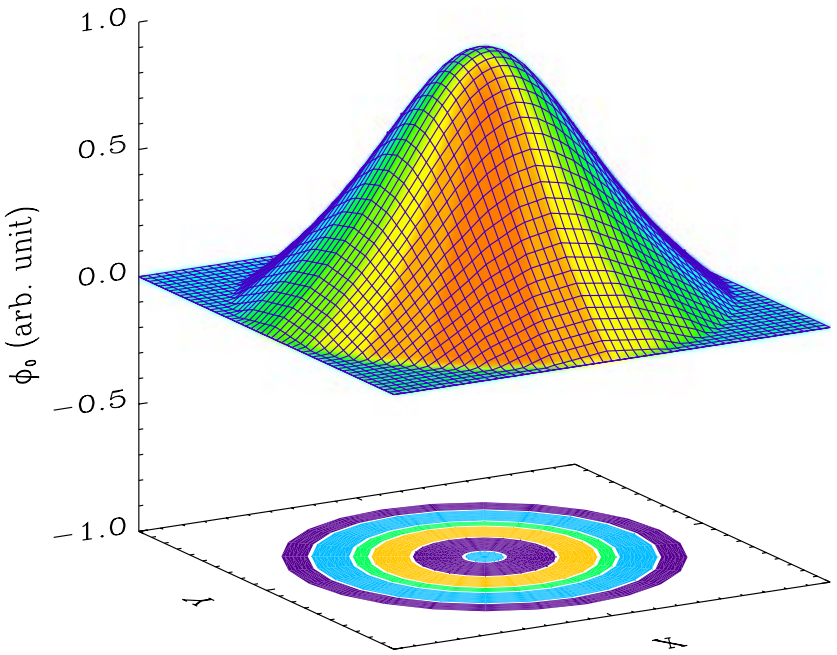

(b) Equilibrium Space-Charge Potential

➪ Equilibrium solutions (ϕ_0, A_{z0}, f_{j0}) solve the steady-state ($\partial/\partial t = 0$) Vlasov-Maxwell equations with $\partial/\partial z = 0$ and $\partial/\partial\theta = 0$.

Nonlinear Properties of Stable Proton Beam Propagation

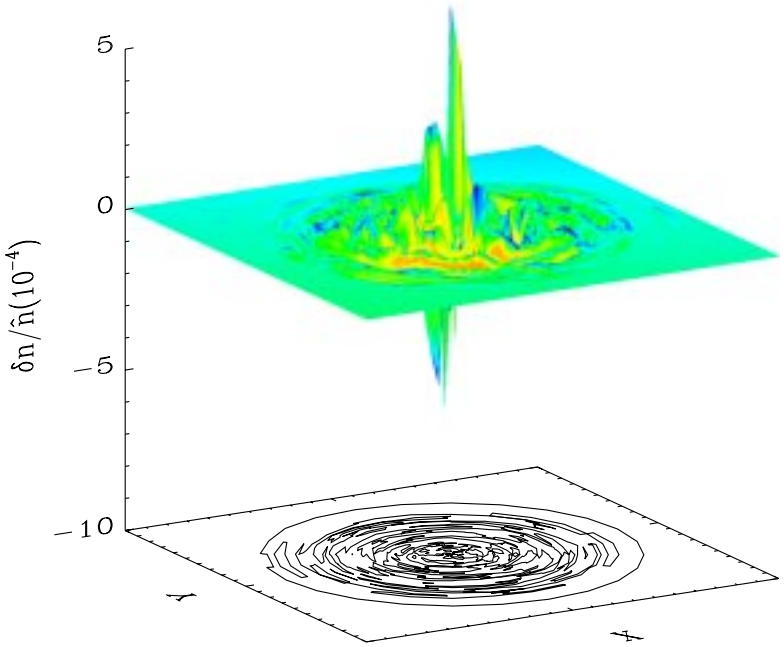

(a) Perturbed δn at $t = 0\tau_\beta$.

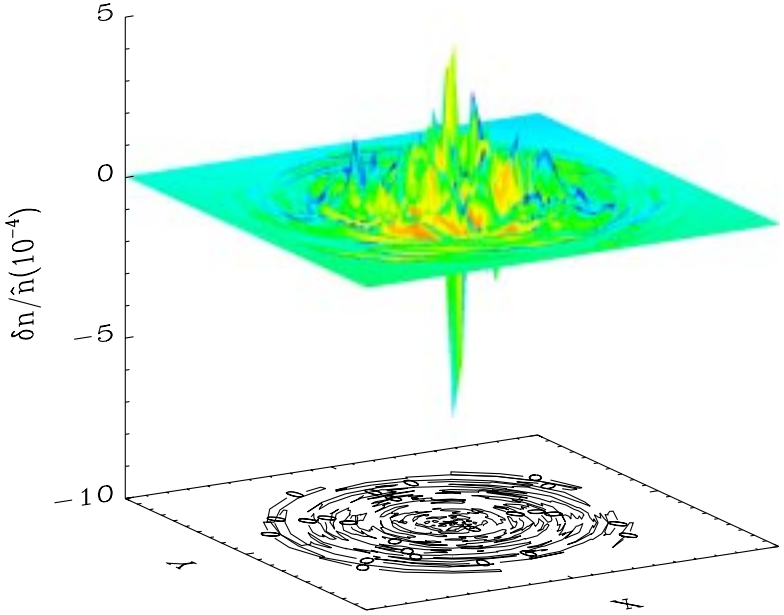

(b) Perturbed δn at $t = 3000\tau_\beta$.

- Random initial perturbation with normalized amplitudes of 10^{-3} are introduced into the system.
- The beam is propagated from $t = 0$ to $t = 3000\tau_\beta$, where $\tau_\beta \equiv \omega_{\beta b}^{-1}$.

Nonlinear Properties of Stable Proton Beam Propagation

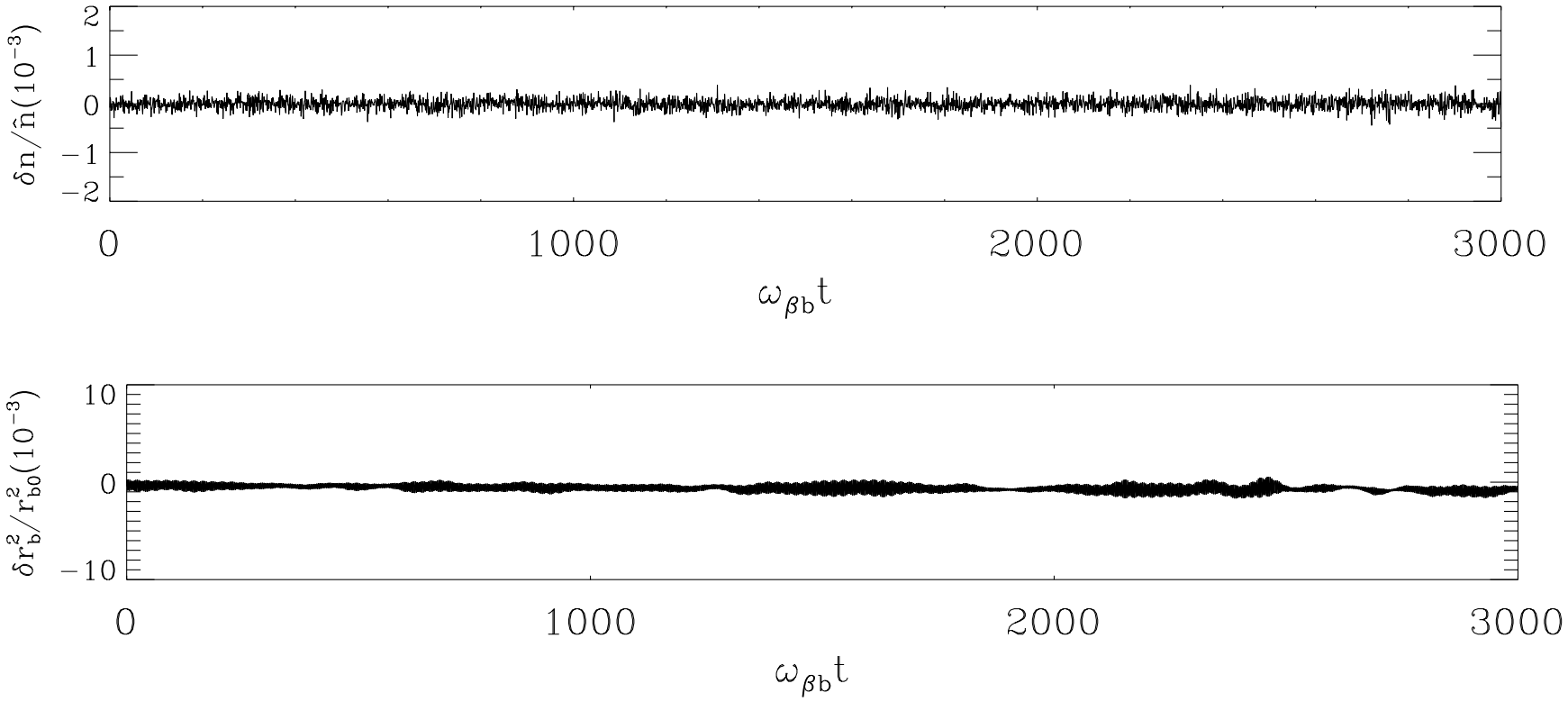

➪ Simulation results show that the perturbations do not grow and the beam propagates quiescently, which agrees with the nonlinear stability theorem for the choice of thermal equilibrium distribution function [PRL **81**, 991 (1998)].

Body Modes by the BEST code

- Axisymmetric body modes with $l = 0$ and $k_z = 0$ for a moderate-intensity beam with $s_b \equiv \hat{\omega}_{pb}^2 / 2\gamma_b^2 \omega_{\beta b}^2 = 0.44$.
- First four body eigenmodes of the system at frequencies $\omega_1 = 1.53\ \omega_{\beta b}$, $\omega_2 = 2.98\ \omega_{\beta b}$, $\omega_3 = 4.50\ \omega_{\beta b}$, and $\omega_4 = 6.03\ \omega_{\beta b}$.
- Eigenfunction $\delta\phi_n(r)$ has n zeros when plotted as a function of r.

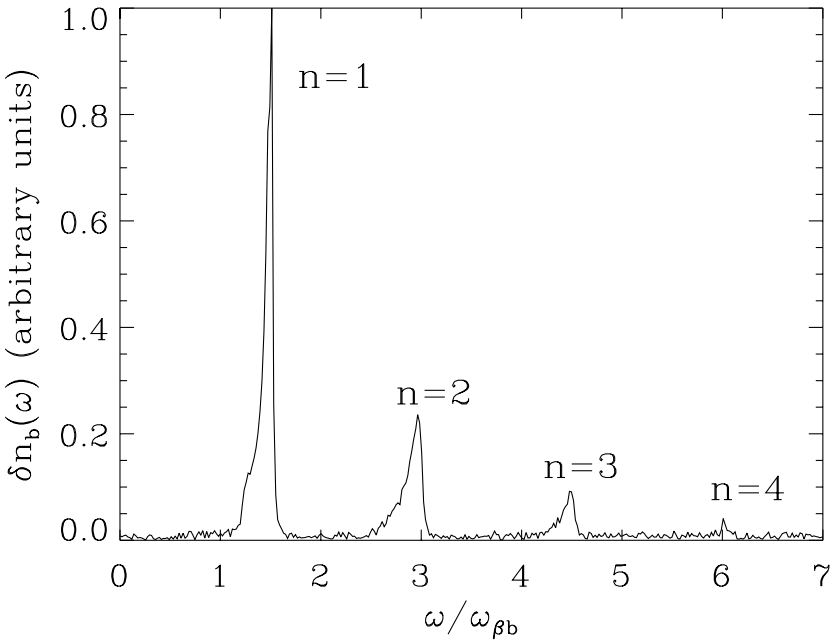

(a) Frequency spectrum

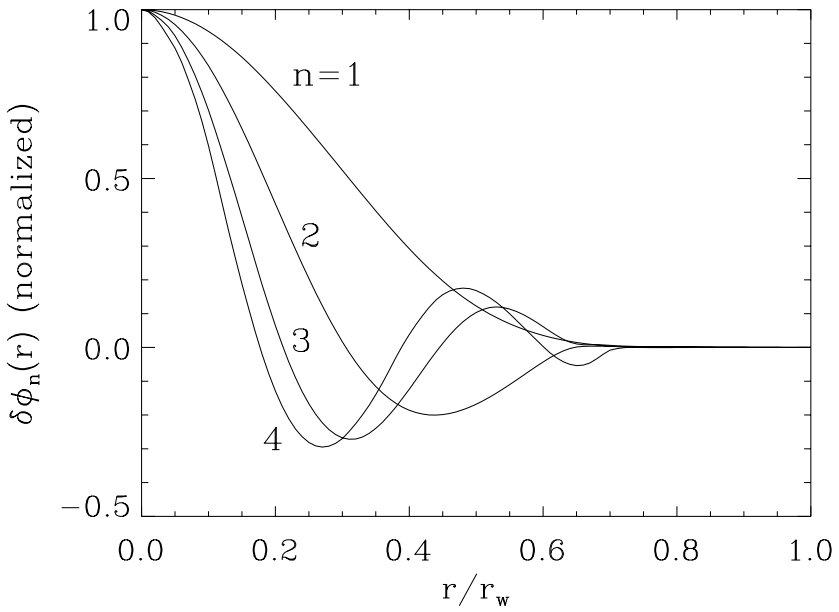

(b) Radial mode structure

Surface Modes

- Linear surface modes for perturbations about a thermal equilibrium beam in the space-charge-dominated regime, with flat-top density profile.

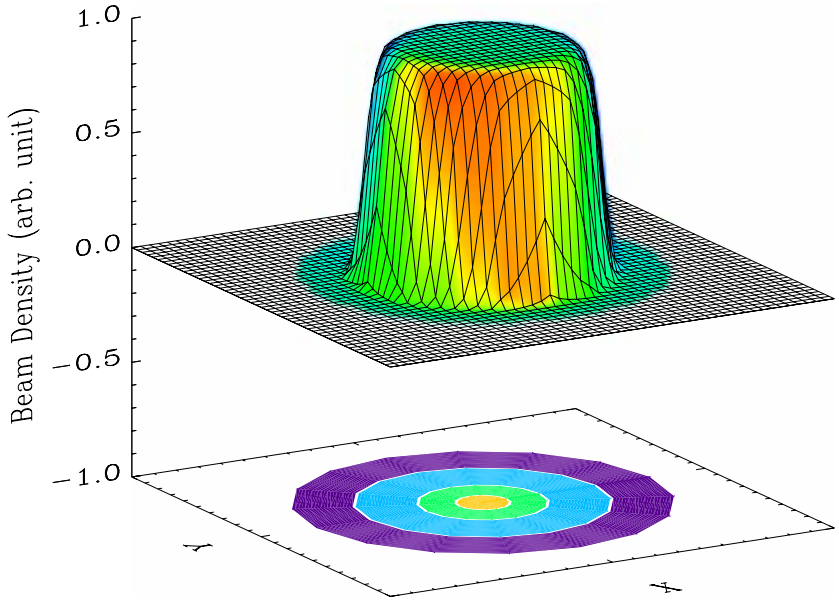

(a) Equilibrium Density

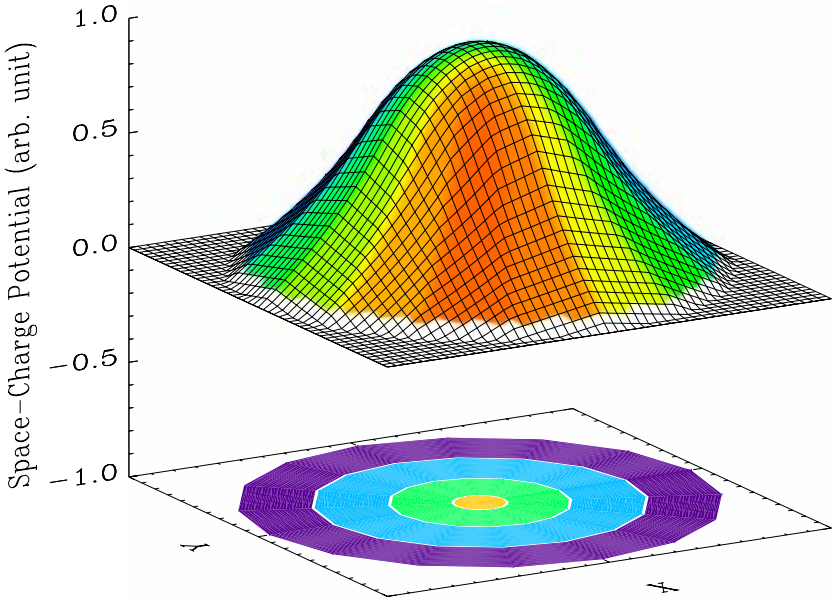

(b) Equilibrium Space-Charge Potential

Surface Modes

- The surface modes can be destabilized by the electron-ion two-stream interaction when background electrons are present.
- The BEST code, operating in its linear stability mode, has recovered well-defined eigenmodes which agree with theoretical predications.

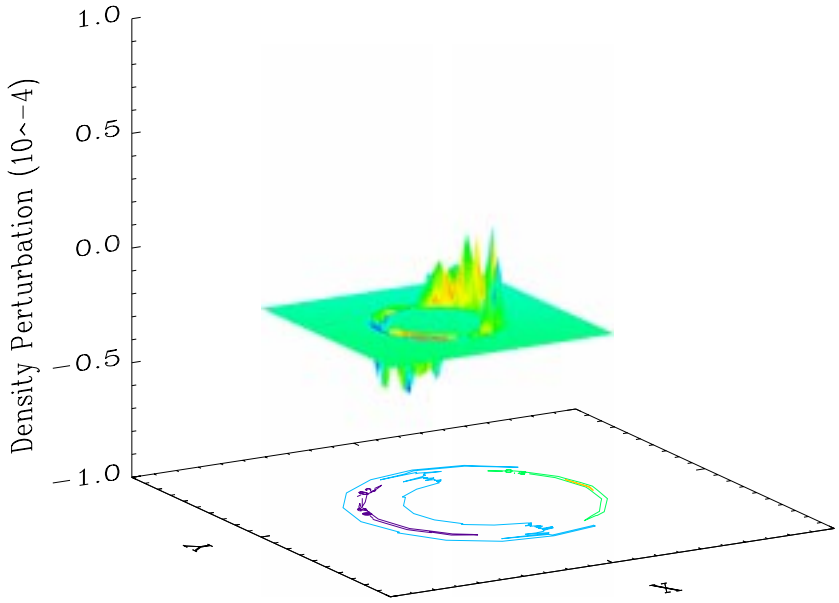

(a) Density Perturbation.

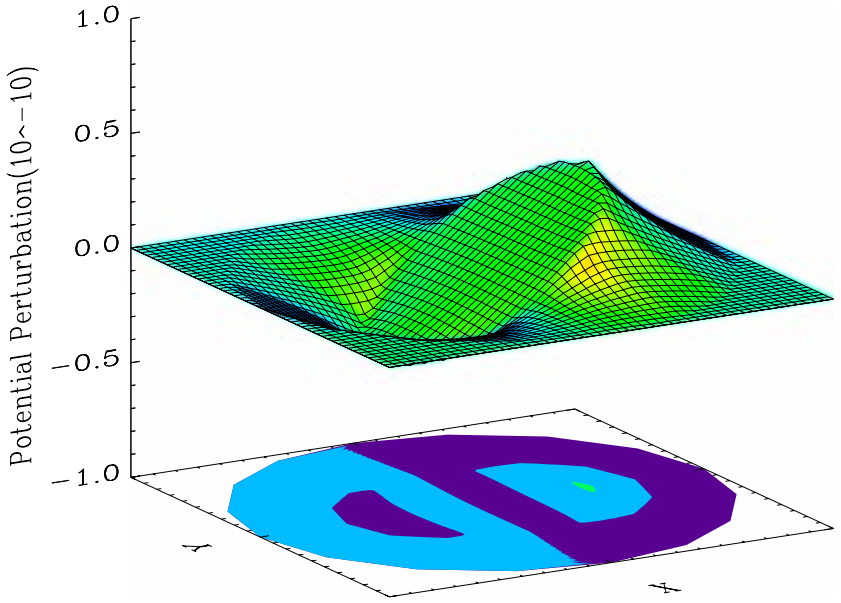

(b) Potential Perturbation.

$l = 1$ Eigenmode in a Moderate-Intensity Proton Beam

- Generally, these is no analytical description of the eigenmodes in beams with nonuniform density profiles.
- However, numerical result shows that eigenmode is localized in the region where the density gradient is large.

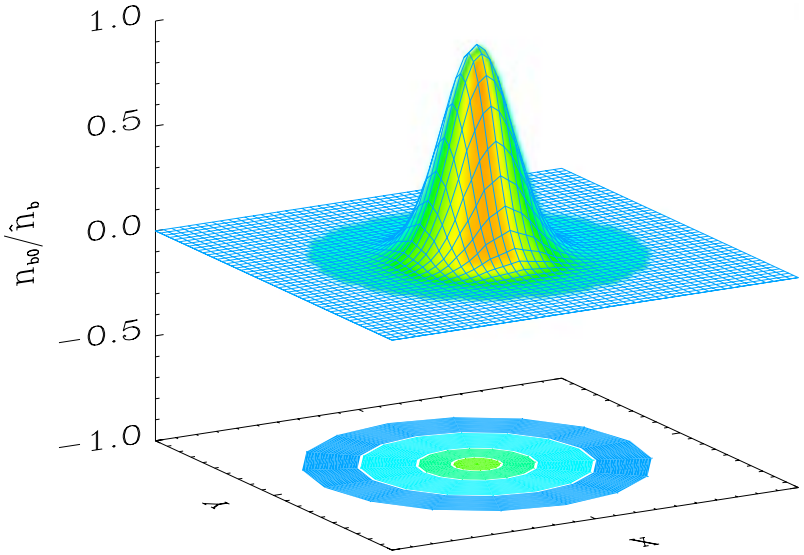

(a) Equilibrium Density Profile

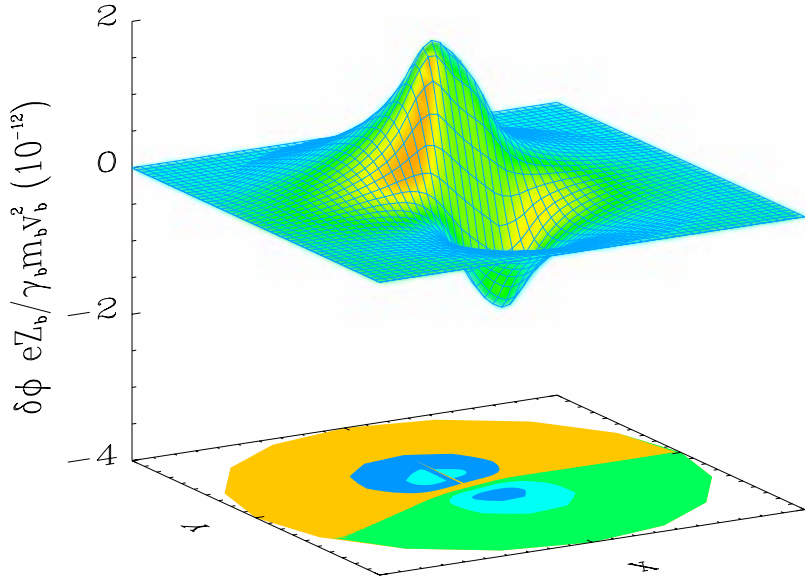

(b) Mode Structure

Surface Modes

- For azimuthal mode number $l = 1$, the dispersion relation is given by

$$\omega = k_z V_b \pm \frac{\hat{\omega}_{pb}}{\sqrt{2}\gamma_b}\sqrt{1 - \frac{r_b^2}{r_w^2}} \tag{1}$$

where r_b is the radius of the beam edge, and r_w is location of the conducting wall. Here, $\hat{\omega}_{pb}^2 = 4\pi\hat{n}_b e_b^2/\gamma_b m_b$ is the ion plasma frequency-squared, and $\hat{\omega}_{pb}/\sqrt{2}\gamma_b \backsimeq \omega_{\beta b}$ in the space-charge-dominated limit.

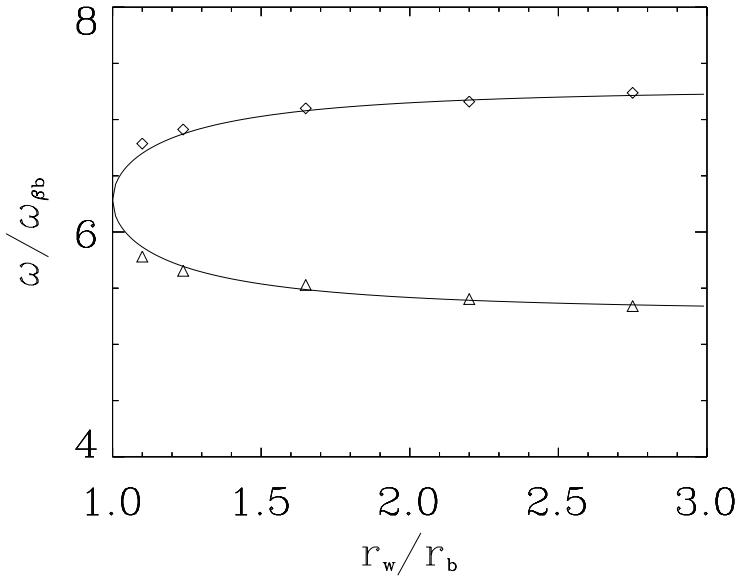

(a) $\omega/\omega_{\beta b}$ versus r_w/r_b

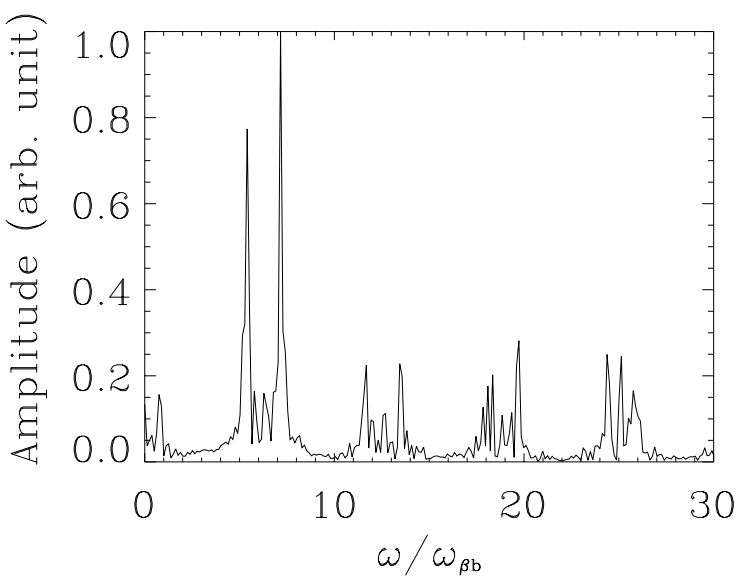

(b) Spectrum for $r_w/r_b = 2.2$

Electron-Proton Two-Stream Instability

- When a background electron component is introduced with $\beta_e = V_e/c \backsimeq 0$, the $l = 1$ "surface mode" can be destabilized for a certain range of axial wavenumber and a certain range of electron temperature T_e.

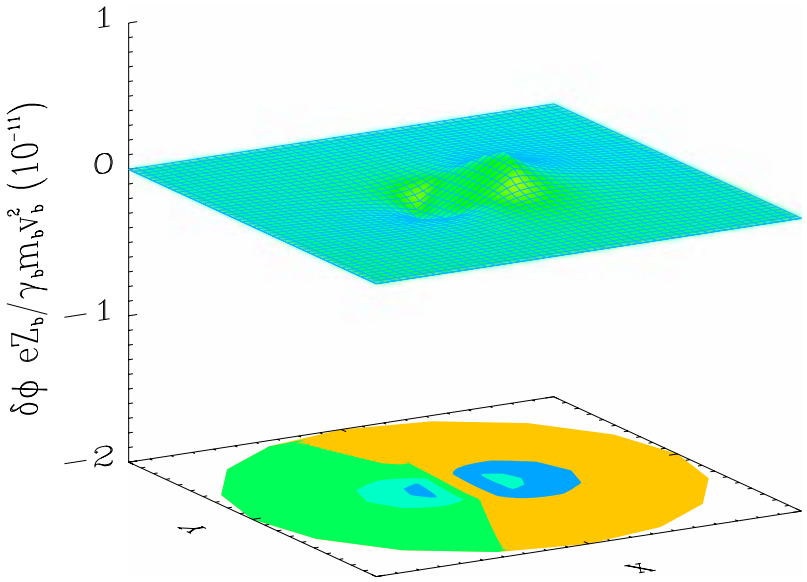

(a) $t = 0$

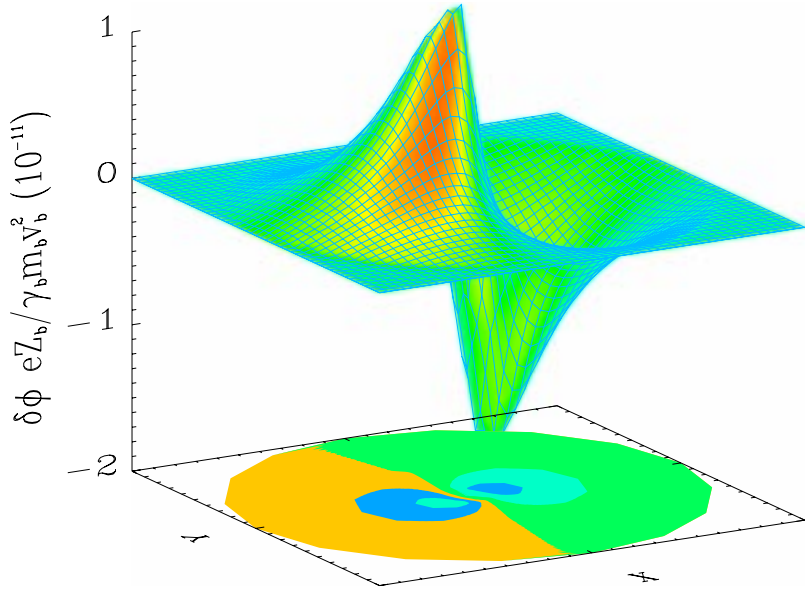

(b) $t = 200/\omega_{\beta b}$

Simulations of e-p Instability for PSR

- Illustrative PSR parameters:
  - Space-charge-induced tune shift: $\delta\nu/\nu_0 \sim -0.020$, $\hat{\omega}_{pb}^2/2\gamma_b^2\omega_{\beta b}^2 = 0.079$.
  - Oscillation frequency (simulations): $f \sim 163$MHz. Mode number at maximum growth $n = 55 \sim 65$.
  - Line densities: $\lambda_b = 9.13 \times 10^8 \mathrm{cm}^{-1}$, $\lambda_e = 9.25 \times 10^7 \mathrm{cm}^{-1}$, $T_{b\perp} = 4.41$keV, $T_{e\perp} = 0.73$keV, $\phi_0(r_w) - \phi_0(0) = -3.08 \times 10^3$Volts.
- Mode number dependence ($k_z = 2\pi n/L = n/R$, R =ring radius):
  - Only for a certain range of $nV_b/\omega_{\beta b}R$ can the collective mode of the beam ions effectively resonate with the electrons and produce instability.
  - For instability, electrons must physically overlap the region of the excited eigenmode.
  - Transverse electron energy distribution determines the radial extent of the electron density profile.

Simulations of e-p Instability for PSR

- System parameters: $\hat{\omega}_{pb}^2/2\gamma_b^2\omega_{\beta b}^2 = 0.079$, $T_{b\perp}/\gamma_b m_b V_b^2 = 3.61 \times 10^{-6}$, and $f = \hat{n}_e/\hat{n}_b = 0.1$. For the Proton Storage Ring (PSR) with $\gamma_b = 1.85$, $\omega_{\beta b} = 4.07 \times 10^7/\text{s}$, the illustrative simulation parameters are:
  $r_w = 5.0\text{cm}$, $r_b = 1.7\text{cm}$, $r_e = 2.15\text{cm}$, $\hat{n}_b = 2.16 \times 10^8\text{cm}^{-3}$,
  $N_b = 9.13 \times 10^8\text{cm}^{-1}$, $N_e = 9.25 \times 10^7\text{cm}^{-1}$,
  $T_{b\perp} = 4.41\text{Kev}$, $T_{e\perp} = 0.73\text{Kev}$, $\phi_0(r_w) - \phi_0(0) = -3.08 \times 10^3\text{Volts}$.

- $k_z V_b/\omega_{\beta b}$ dependence ($k_z = 2\pi n/L = n/R$, R =ring radius):
  - Only for a certain range of $k_z V_b/\omega_{\beta b}$ can the collective mode of the beam ions effectively resonate with the electrons and produce instability.

- $T_{e\perp}/T_{b\perp}$ dependence:
  - For instability, electrons must physically overlap the region of the eigenmode.
  - Electrons are radially confined by the space charge potential of the beam ions.
  - Transverse electron temperature determines the radial extent of the electron density profile.

Instability Growth Rate with $T_{e\|} = T_{b\|} = 0$

➪ The $k_z V_b/\omega_{\beta b}$ and $T_{e\perp}/T_{b\perp}$ dependences of the growth rate are qualitatively consistent with the analytical results obtained for uniform-density beams.

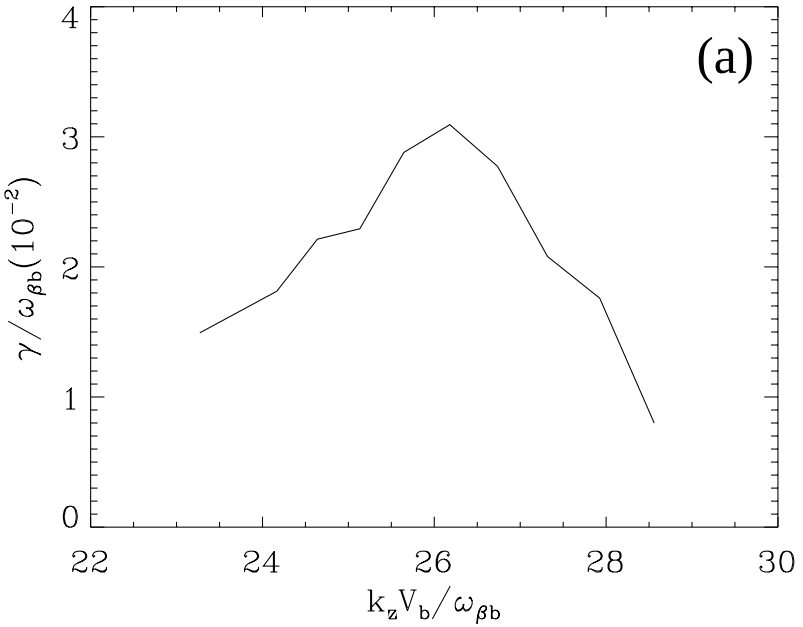

(a) γ versus $k_z V_b/\omega_{\beta b}$

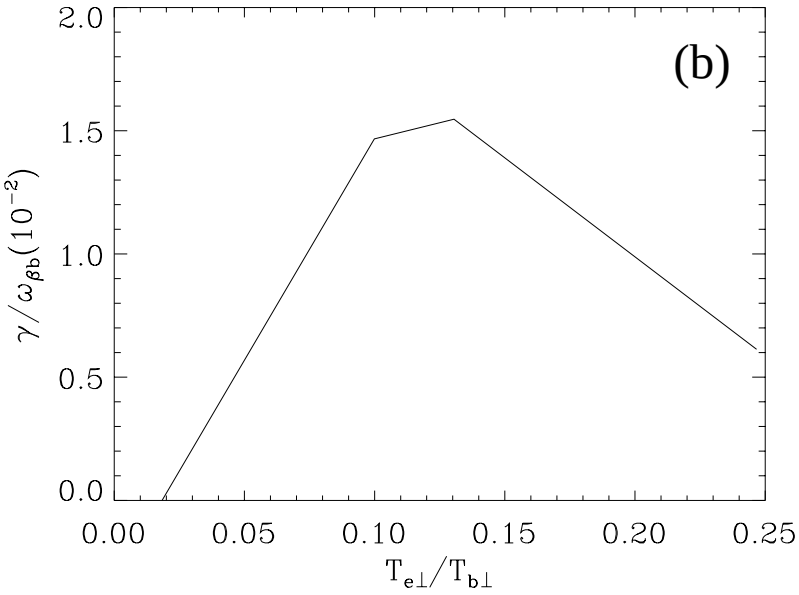

(b) γ versus $T_{e\perp}/T_{b\perp}$

Cold Electrons with $T_{e\perp}/T_{b\perp} = 0.018$, $T_{e\parallel} = T_{b\parallel} = 0$

- Electrons are relatively cold and localized in the beam center, and no instability developed over $370\omega_{\beta b}^{-1}$.

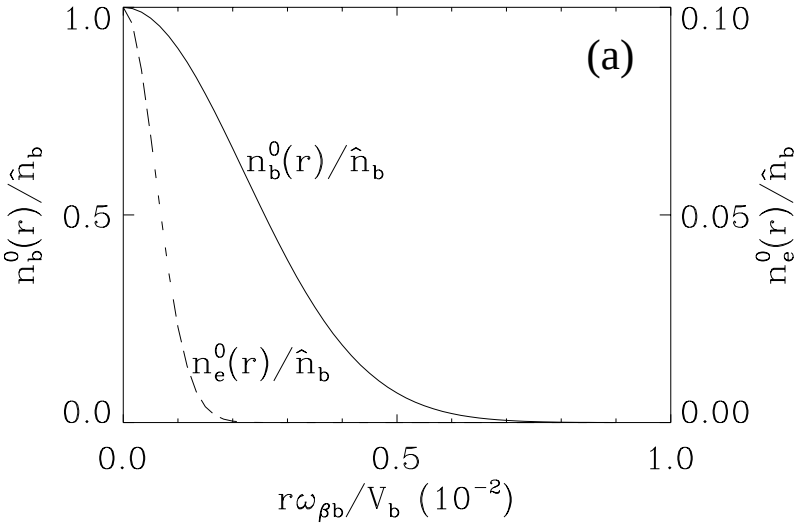

(a) Equilibrium Density

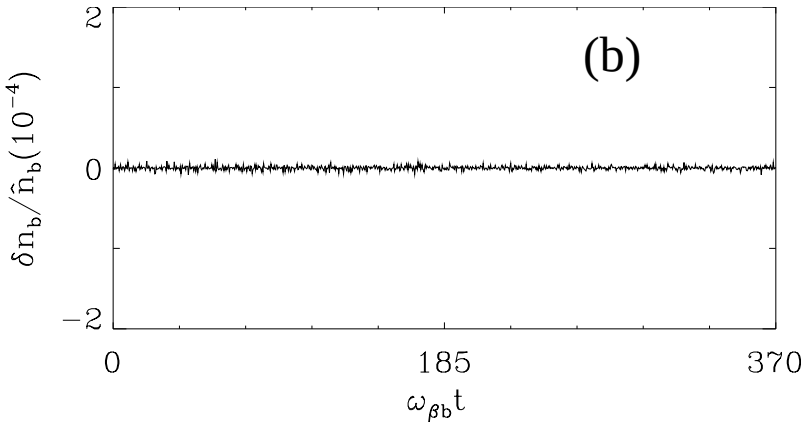

(b) Perturbation Time History

Warm Electrons with $T_{e\perp}/T_{b\perp} = 0.13$, $T_{e\|} = T_{b\|} = 0$

- Electrons are sufficiently hot that the electron density profile overlaps that of the beam ions, and the onset of a strong e-p instability is observed.

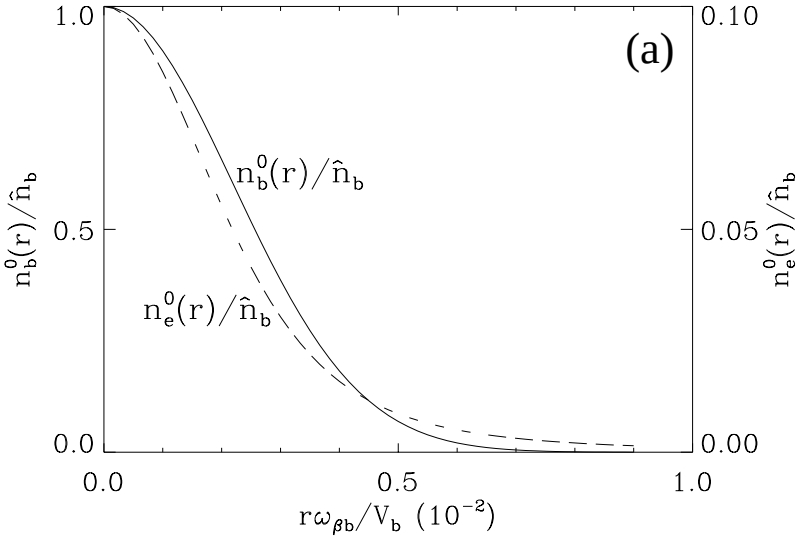

(a) Equilibrium Density

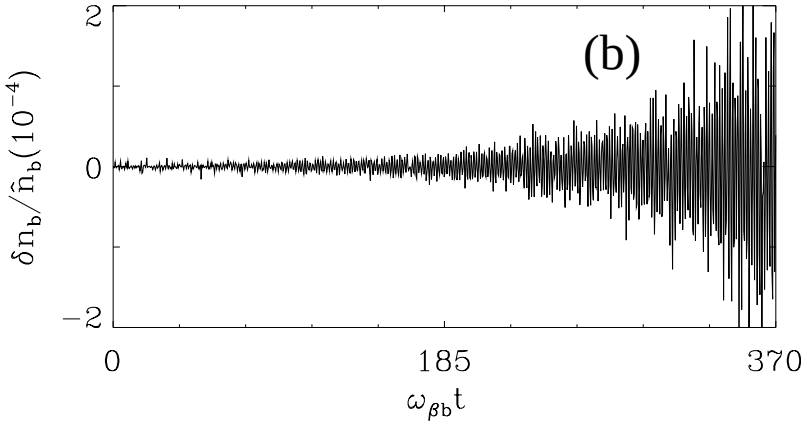

(b) Perturbation Time History

Growth Rate for Illustrative PSR Parameters

- Maximum growth rate depends on the normalized beam density $\hat{n}_b/\hat{n}_{b0}$ and the initial axial momentum spread.

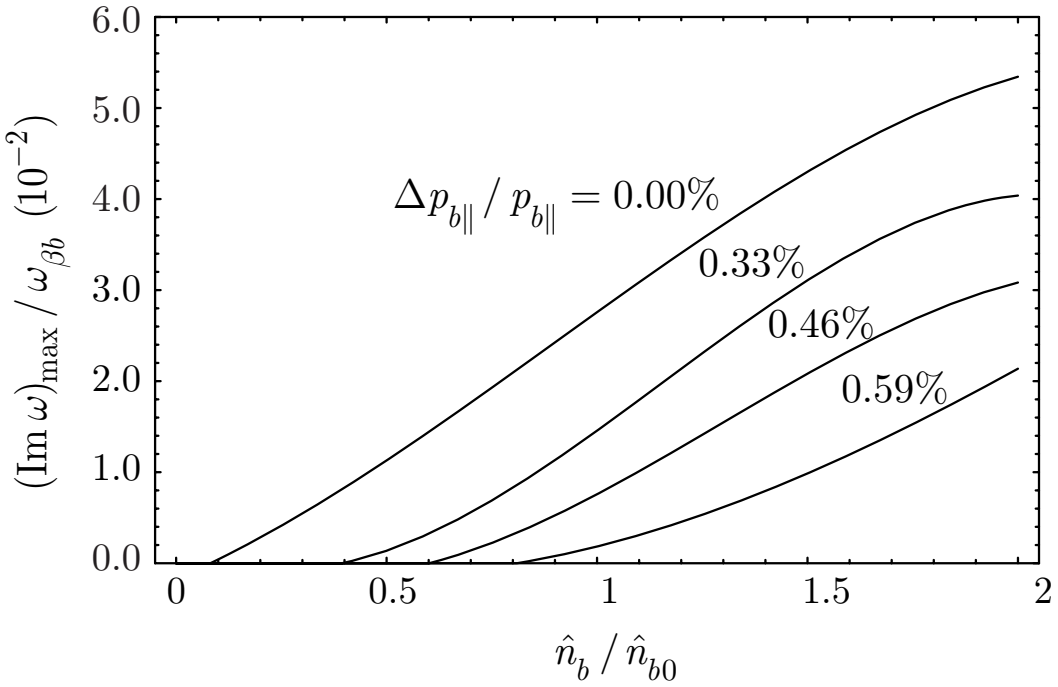

- $\hat{n}_{b0} = 9.41 \times 10^8 \mathrm{cm}^{-3}$, corresponding to an average current of 35 A in the PSR experiment ($\hat{\omega}_{pb}^2/2\gamma_b^2\omega_{\beta b}^2 = 0.079$).

- A larger longitudinal momentum spread induces stronger Landau damping by parallel kinetic effects and therefore reduces the growth rate of the instability.

- Higher beam intensity provides more free energy to drive a stronger instability.

Instability Threshold for Illustrative PSR Parameters

- Important damping mechanisms includes
  - Longitudinal Landau damping by the beam ions.
  - Stabilizing effects due to space-charge-induced tune spread.
- An instability threshold is observed in the simulations.

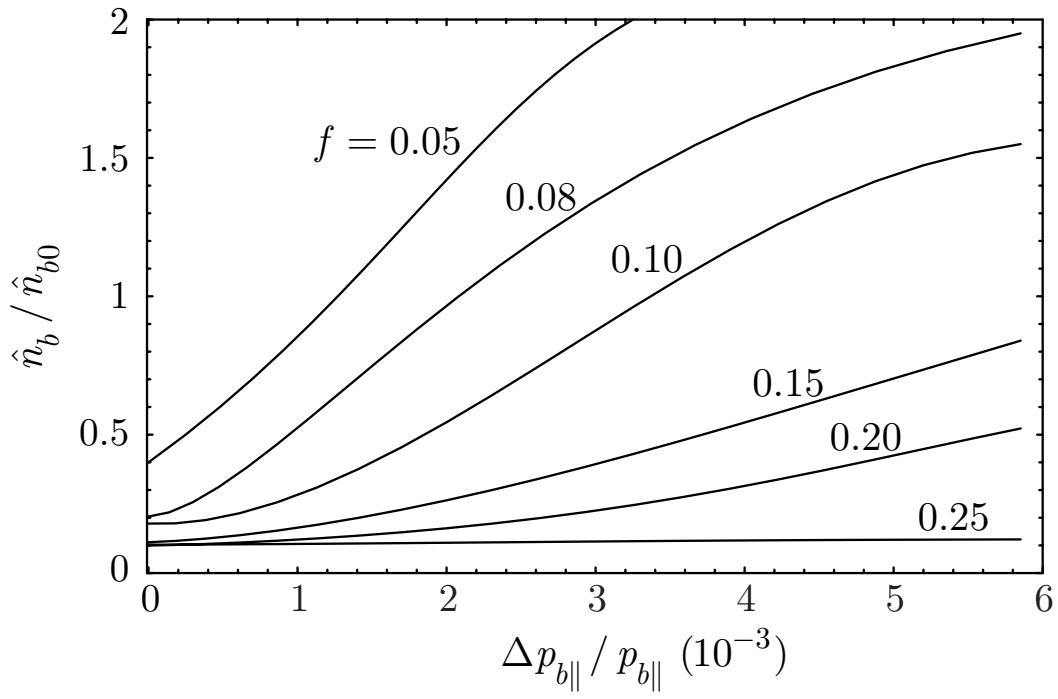

- Larger momentum spread and smaller fractional charge neutralization imply a higher density threshold for the instability to occur.

Long-Time Evolution of the e-p Instability

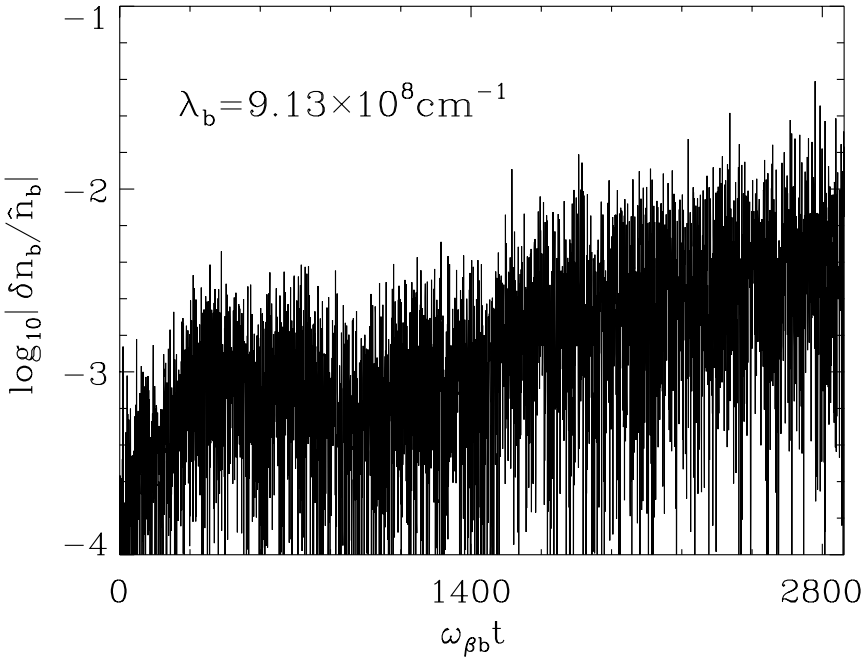

- Late-time nonlinear phase of e-p instability.
- Late-time nonlinear growth observed for system parameters above marginal stability.
- Simulations show two phases to the e-p instability.

Long-Time Evolution of the e-p Instability

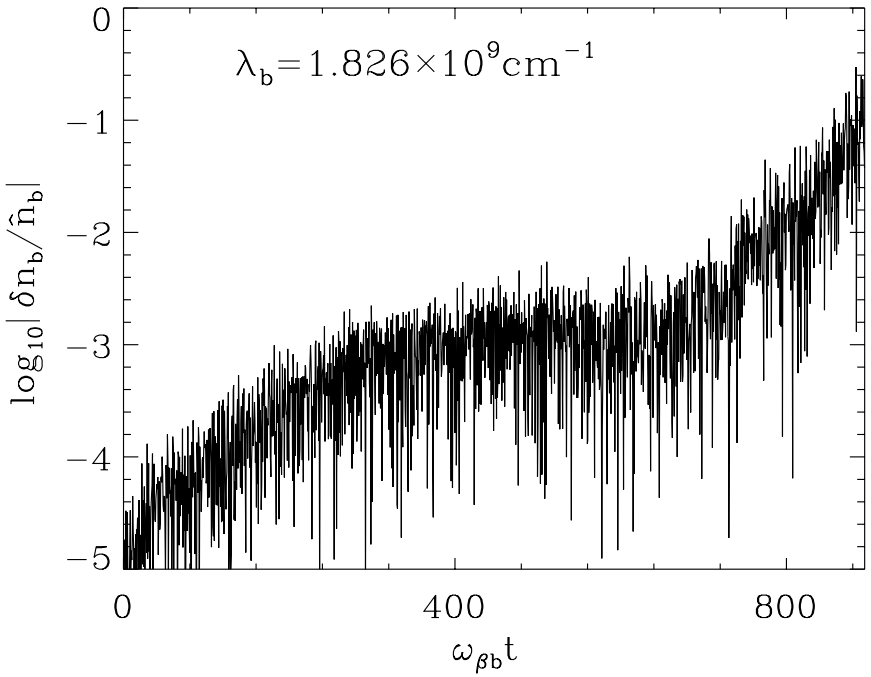

- Late-time nonlinear phase of e-p instability at twice the beam intensity.
- Nonlinear growth to larger amplitudes occurs on faster time scale.

Conclusions

- A 3D multispecies nonlinear perturbative particle simulation method has been developed to study two-stream instabilities in intense charged particle beams described self-consistently by the Vlasov-Maxwell equations.
- Introducing a background component of electrons, the two-stream instability is observed in the simulations. Several properties of this instability are investigated numerically, and are found to be in qualitative agreement with theoretical predictions.
- For PSR parameters, the self-consistent simulations show that the e-p instability has a dipole mode structure, and the growth rate is an increasing function of proton density and fractional charge neutralization.
- For PSR parameters, the simulations show that an axial momentum spread and the space-charge induced tune spread provide effective stabilization mechanisms for the e-p instability.
- Large scale parallel simulations have been carried out to determine scaling properties of e-p instability with beam intensity and fractional charge neutralization.

Conclusions

- The BEST code, a 3D multispecies perturbative particle simulation code, has been tested and applied in different operating regimes.
- Simulation particles are used to follow only the perturbed distribution function and self-fields. Therefore, the simulation noise is reduced significantly.
- Perturbative approach also enables the code to investigate different physics effects separately, as well as simultaneously.
- The BEST code can be easily switched between linear and nonlinear operation, and used to study both linear stability properties and nonlinear beam dynamics.
- These features provide PSR with very effective tool to investigate the electron-proton two-stream instability, halo formation, and many other key problems in nonlinear beam dynamics and accelerator physics.

PPPL PRINCETON PLASMA PHYSICS LABORATORY

Studies of Two-Stream Instability – Future Plans

- **Understand nonlinear dynamics** of the two-stream instability, including mode saturation, stabilization mechanisms, and ion and electron dynamical response.

- Identify operating regimes for PSR and SNS that minimize the deleterious effects of the two-stream instability and maximize the threshold beam intensity for the onset of the two-stream instability.

Nonlinear δf Particle Simulation with Self-field, Chromaticity, and Slip Factor

- Particle dynamics including self-field, chromaticity, and slip factor.

$$
\begin{aligned}
\frac{d\boldsymbol{x}_\perp}{dt} &= (\gamma_j m_j)^{-1}\boldsymbol{p}_\perp \\
\frac{d\boldsymbol{p}_\perp}{dt} &= -\gamma_j m_j(1+\frac{\xi_j\delta p_z}{p_{z0j}})^2\omega_{\beta j}^2\boldsymbol{x}_\perp - e_j(\nabla_\perp\phi - \frac{v_z}{c}\nabla_\perp A_z) \\
\frac{dz}{dt} &= V_j + (\frac{1}{\gamma_j^2} - \frac{1}{\gamma_{tj}^2})\frac{1}{\gamma_j m_j}\delta p_z \\
\frac{dp_z}{dt} &= -e_j\nabla_\parallel\phi
\end{aligned}
$$

- Weight functions w_j are carried by the simulation particles, and the dynamical equations for w_j are derived from the definition of w_j and the Vlasov equation.

$$
\begin{aligned}
\frac{dw}{dt} &= -(1-w)\frac{1}{f_{j0}}\frac{\partial f_{j0}}{\partial \boldsymbol{p}} \cdot \delta\left(\frac{d\boldsymbol{p}}{dt}\right) \\
\delta\left(\frac{d\boldsymbol{p}}{dt}\right) &\equiv -e_j(\nabla\delta\phi - \frac{v_z}{c}\nabla_\perp \delta A_z)
\end{aligned}
$$

Electromagnetic Simulation Using Darwin Model

- Darwin model ignores the transverse displacement current to eliminate fast light waves.

- Nonlinear Vlasov-Maxwell equations in the six-dimensional phase space $(\boldsymbol{x}, \boldsymbol{p})$:

$$\left\{ \frac{\partial}{\partial t} + \boldsymbol{v} \cdot \frac{\partial}{\partial \boldsymbol{x}} - [\gamma_j m_j \omega_{\beta j}^2 \boldsymbol{x}_\perp + e_j (\nabla \phi - \frac{p_{zj}}{\gamma_j m_j c} \nabla_\perp A_z + \frac{1}{c} \frac{\partial A_z}{\partial t} \hat{\boldsymbol{e}}_z)] \cdot \frac{\partial}{\partial \boldsymbol{p}} \right\} f_j(\boldsymbol{x}, \boldsymbol{p}, t) = 0$$

and

$$\nabla^2 \phi = -4\pi \sum_j e_j \int f_j(\boldsymbol{x}, \boldsymbol{p}, t)\ d^3p$$

$$\nabla^2 A_z = -\frac{4\pi}{c} \sum_j e_j \int v_z f_j(\boldsymbol{x}, \boldsymbol{p}, t)\ d^3p$$

Electromagnetic Simulation Using Darwin Model

- Equations of motion for the particles are given by

$$\begin{aligned}
\frac{d\boldsymbol{x}_{ji}}{dt} &= (\gamma_j m_j)^{-1}\boldsymbol{p}_{ji} \\
\frac{d\boldsymbol{p}_{ji}}{dt} &= -\gamma_j m_j \omega_{\beta j}^2 \boldsymbol{x}_{\perp ji} - e_j(\nabla\phi - \frac{p_{zj}}{\gamma_j m_j c}\nabla_\perp A_z + \frac{1}{c}\frac{\partial A_z}{\partial t}\hat{\boldsymbol{e}}_z)
\end{aligned}$$

- To eliminate the numerical instability associated with the $\partial A_z/\partial t$ term, p_{zj} is advanced through the "canonical momentum" $P_{zj} \equiv p_{zj} + e_j \delta A_z/c$.

$$\begin{aligned}
\frac{dP_{zji}}{dt} &= -e_j[\frac{\partial\phi}{\partial z} - \frac{1}{c\gamma_j m_j}(P_{zj} - e_j\delta A_z/c)\frac{\partial A_z}{\partial z}] \\
\nabla^2\delta A_z &= -4\pi\sum_j \int \frac{e_j P_{zj}}{\gamma_j m_j c}\delta f_j(\boldsymbol{x},\boldsymbol{p},t)\ d^3\boldsymbol{p} + 4\pi\sum_j \frac{e_j^2 n_j}{\gamma_j m_j c}\delta A_z \\
p_{zji} &= P_{zji} - e_j\delta A_z/c
\end{aligned}$$

References

[1]R. C. Davidson, *Physics of Nonneutral Plasmas* (Addison-Wesley Publishing Co., Reading, MA, 1990), and references therein.

[2]A. W. Chao, *Physics of Collective Beam Instabilities in High Energy Accelerators* (Wiley, New York, 1993).

[3]See, for example, Proceedings of the 1997 International Symposium on Heavy Ion Inertial Fusion (Ed., I. Hofmann), Nuclear Instruments and Methods in Physics Research **A 415**, pp. 1-508 (1998), and references therein.

[4]R. C. Davidson, Physics of Plasmas **5**, 3459 (1998).

[5]R. C. Davidson, Physical Review Letters **81**, 991 (1998).

[6]R. C. Davidson and C. Chen, Particle Accelerators **59**,175 (1998).

[7]R. C. Davidson, H. Qin, and P. J. Channell, Physical Review Special Topics on Accelerators and Beams **2**, 074401 (1999); P. J. Channell, Physics of Plasmas **6**, 982 (1999).

[8]W. W. Lee, Q. Qian, and R. C. Davidson, Physics Letters A **230**, 347 (1997); Q. Qian, W. W. Lee, and R. C. Davidson, Physics of Plasmas **4**, 1915 (1997).

[9]P. H. Stoltz, R. C. Davidson, and W. W. Lee, Physics of Plasmas **6**, 298 (1999).

[10]H. Qin, R. C. Davidson, and W. W. Lee, Proceedings of the 1999 Particle Accelerator Conference **3**, 1626 (1999).

[11]S. M. Lund and Davidson, Physics of Plasmas **5**, 3028 (1998).

[12]R. C. Davidson and S. Strasburg, Physics of Plasmas **7**, in press (2000).

[13]R. C. Davidson, H. Qin, P. H. Stoltz, and T. -S. Wang, Physical Review Special Topics on Accelerators and Beams **2**, 054401 (1999), and references therein.

[14]R. C. Davidson, H. Qin, and T. -S. Wang, Physics Letters A **252**, 213 (1999).

[15]D. Neuffer, E. Colton, D. Fitzgerald, T. Hardek, R. Hutson, R. Macek, M. Plum, H. Thiessen, and T. -S. Wang, Nucl. Instr. Methods Phys. Res. **A321**, 1 (1992).

[16]R. Macek, Proceeding of Workshop on Space Charge Physics in High Intensity Hadron Rings, American Institute of Physics Conference Proceedings **448**, 116 (1998).

[17]H. Qin, R. C. Davidson, and W. W. Lee, Physical Review Special Topics – Accelerators and Beams **3**, 084401 (2000).

[18]H. Qin, R. C. Davidson, and W. W. Lee, Physics Letters A **272**, 389 (2000).

[19]S. M. Lund, *et al*, Proceeding of the 19th International Linac Conference (Chicago, Illinois, 1998).

[20]R. C. Davidson and H. Qin, Physics Letters A **270**, 177 (2000).

[21]R. C. Davidson, H. Qin, I. Kaganovich, and W. W. Lee, Proceeding of the 13th International Symposium on Heavy Ion Inertial Fusion (San Diego, CA, 2000).